

# Measurement of Structural Deformation using Terrestrial Laser Scanners

Stuart GORDON, Derek LICHTI, Jochen FRANKE and Mike STEWART, Australia

**Key words:** deformation measurement, laser scanning, modelling.

## SUMMARY

Three deformation measurement experiments have been undertaken where, in each experiment, a structure was subject to controlled loading. Terrestrial laser scanners (TLSs) were used to make measurements at critical intervals during each load test. TLSs, which are a relatively recent innovation, are capable of rapidly capturing thousands of three dimensional points over the surface of an object. They are largely untried in the area of structural deformation monitoring. The purpose of these tests is to assess the sensitivity of TLSs for the measurement of vertical deformation of loaded structures and to investigate their potential for metrology tasks where remote observations (completely non-contact and targetless at distances greater than 5m) are desirable.

A Riegl LMS-Z210 laser scanner was used for all three experiments and a Cyra Cyrax 2500 was available for the first. The point cloud data were represented with analytical models representing the vertical deflection of each beam. The development of these models required knowledge of the dimensions of the beam, spatial position of the load point(s) and support points. Functional models (low-order polynomials) were derived based on generalised coefficients of the analytical models. These generalised coefficients were solved as unknown parameters in a least-squares estimation process.

Analysis of the accuracy of the TLSs involved computing differences between benchmark photogrammetry and laser scanner vertical deflections. In the first experiment, the RMS of differences (for eight load cases) between the Cyrax 2500 and photogrammetry was  $\pm 0.29\text{mm}$  and  $\pm 3.6\text{mm}$  for the LMS-Z210 (using 104 samples). The RMS of differences for the LMS-Z210 in the second experiment was  $\pm 2.4\text{mm}$  for 12 load cases (using 144 samples). The RMS of differences for the final experiment, where measurements were conducted on four horizontal beams, ranged between  $\pm 4.2\text{mm}$  to  $\pm 9.5\text{mm}$ . The greatest improvement of accuracy was up to 21 times the single-point precision of the TLS. These results highlight the potential application of TLSs for precision metrology, given that their accuracy can be greatly improved by exploiting the 3D point clouds with simple modelling techniques.

# Measurement of Structural Deformation using Terrestrial Laser Scanners

Stuart GORDON, Derek LICHTI, Jochen FRANKE and Mike STEWART, Australia

## 1. INTRODUCTION

Terrestrial laser scanners (TLSs) are modern geomatic data capture instruments that offer numerous measurement benefits including three-dimensional data capture, remote and non-contact (i.e. targetless) operation, a permanent visual record and dense data acquisition. TLSs are currently being used in a variety of projects, including heritage mapping, as-built documentation and topographic surveys. However, the precision of TLSs is not perceived adequate for industrial metrology applications, such as deformation monitoring.

The advantage of TLSs is that, although individual sample points are low in precision (e.g.  $\pm 2\text{mm}$  to  $\pm 50\text{mm}$ ), modelling of the entire point cloud may be effective for representing the change of shape of a structure. A modelled surface will be a more precise representation of the object than the unmodelled observations. In light of this notion, a methodology for measuring structural deformation, relying on theoretical aspects of beam mechanics and implemented by constrained least-squares curve fitting, has been developed and is presented in Section 2. The results of two structural deformation monitoring experiments, involving beams (one concrete and one timber) being loaded in a load-testing frame, used to test the analytical modelling strategy are presented in Sections 3 and 4. A field case involving the span of a timber bridge is shown in Section 5. All experiments were controlled with convergent digital photogrammetry.

## 2. BEAM DEFLECTION BY INTEGRATION

There are numerous 3D data modelling techniques available, such as creating a TIN or gridding. Selection of an appropriate surface model is critical to permit the accurate computation of an object's deformation. The method chosen to model vertical deflections in these experiments is based on forming analytical models representing the physical bending of the beam. The models are derived from first principles of beam deflection by integration, which essentially yields low order polynomials (no higher than a quadratic in the experiments presented later). Once these models are developed, the coefficients of the polynomials are solved as unknown parameters in a least-squares estimation process. The observations consist of the several hundred 3D point samples from each TLS. A single functional model is used to represent the beam deflection but the parameters of the model are estimated for each deflection epoch.

A beam which is subjected to loading will bend into an arc which can be defined by a curvature function (Beer and Johnston, 1992). The equation, shown in Eq. 1, is a second-order linear differential equation and is composed of the beam's bending moment,  $M$ , which is a function of  $x$ , the distance along the beam, divided by the modulus of elasticity,  $E$ , and moment of inertia,  $I$ . This equation holds true for small deflections. Integrating Eq. 1 twice,

with respect to  $x$ , will yield the function of deflection. This function will permit the vertical deflections to be computed.

$$\frac{\partial^2 z}{\partial x^2} = \frac{M(x)}{EI} \quad (1)$$

The modelling process can be demonstrated using an example. Consider a simply supported beam (i.e. a support point at each of its ends) consisting of a load point,  $P$ , at the centre of the beam, located at  $x_p$ . A sketch is shown in Figure 1.

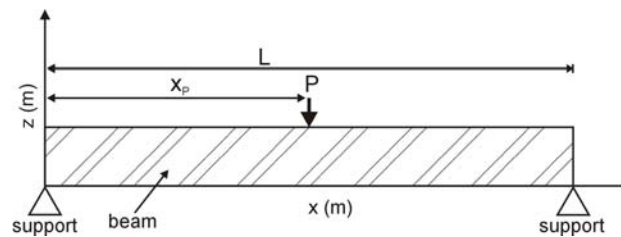


**Figure 1:** Schematic diagram for the timber beam

The bending moment, represented by two functions (one each side of  $x_p$ ), is linear, maximum at  $x_p$  and zero at each support point. Two successive integrations yield a cubic equation. The generalised form of the compound cubic polynomial is given in Eq. 2 and may be adopted for curve fitting the beam shown in Figure 1. An additional term in the  $y$ -axis direction is added to model any linear tilts about the  $x$ -axis ( $\omega$  rotation) that may be evident in the 3D scan cloud of the beam. Justification for this term is given later. A detailed derivation of the model (and curve fitting constraints) can be found in Gordon et al. (2003b).

$$z = \begin{cases} z_1 = a_{30}x^3 + a_{10}x + a_{00} + a_{01}y & ; 0 \leq x \leq x_p \\ z_2 = b_{30}x^3 + b_{20}x^2 + b_{10}x + b_{00} + a_{01}y & ; x_p \leq x \leq L \end{cases} \quad (2)$$

### 3. EXPERIMENT I: TIMBER BEAM

The beam modelling strategy was assessed using two laboratory-based experiments and a field survey. The first experiment involved the controlled loading of a timber beam on an indoor test frame based in the Department of Civil Engineering laboratories at Curtin University. The beam, which had dimensions of 5.0m x 0.2m x 0.1m, was supported at each of its ends. The loading was applied by a hydraulic jack that was positioned at the centre of the beam.

A total of eight load increments were applied whereby a nominal 5mm of vertical displacement (at the centre of the beam) was induced on each occasion. A 'dead load' was collected at the beginning of the testing permitting the capture of a zero-load case. A dial gauge was positioned in the approximate centre of the beam and was used by the jack

operator to assist in determining each 5mm increment (it was not used for analysis). The total downward vertical deflection measured at the centre of the beam was approximately 40mm.

### 3.1 Instrumentation

Two TLSs were used during these experiments: a Cyra Cyrax 2500 (Leica Geosystems, 2004) and a Riegl LMS-Z210 (Riegl, 2004). The Cyrax 2500 is capable of acquiring three-dimensional points at a rate of 1000Hz. The scanner's range precision is  $\pm 4\text{mm}$  ( $1\sigma$ ) and it possesses a coordinate precision of  $\pm 6\text{mm}$  ( $1\sigma$ ). The LMS-Z210 collects points at a rate of 6000Hz. Though faster than the Cyrax 2500, its range precision of  $\pm 25\text{mm}$  ( $1\sigma$ ) is much poorer. Its point coordinate precision, at the distances used in this research ( $<10\text{m}$ ), is commensurate with its range precision (i.e.  $\pm 25\text{mm}$ ).

With respect to imaging resolution, the Cyrax 2500 has a minimum sampling interval of less than 1mm (at 10m) but this resolution is tempered somewhat by a laser beamwidth of approximately 6mm at the same range (Lichti, 2004). The LMS-Z210 has a relatively large beamwidth compared to most commercially available TLSs. The beamwidth is approximately 30mm at 10m and the TLS has a minimum sampling interval of 13mm at 10m. Further information regarding these instruments may be sought from the respective manufacturer's website.

Close-range photogrammetry was used to control both major experiments. A Kodak DC420 with a CCD array of 1524 by 1012 pixels (square pixels with a  $9\mu\text{m}$  width) fitted with a 14mm lens was used. In all cases, the focal ring was set to infinity and secured with tape. The cameras were calibrated before and after each experiment.

### 3.2 Data Collection

The Cyrax 2500 was located 5.4m from the centre of the timber beam and to the left of the laboratory and the LMS-Z210 was positioned 6.4m from the centre of the beam away to the right of the laboratory. Both instruments were set up on stable footings and were not moved for the entire experiment. It was assumed that the TLSs were completely stationary for the duration of the testing, which lasted two hours. Neither instrument was force-centred over a pre-marked known point. The LMS-Z210 was levelled but the Cyrax 2500 was not (it does not have a level bubble).

During loading, high-resolution scans were collected at each epoch by each of the scanners. The Cyrax 2500, which has a relatively slower data capture rate than the LMS-Z210, only acquired a single scan per load epoch. The LMS-Z210, which offers a relatively coarser coordinate precision than the Cyrax 2500, captured three repeat scans of the beam that were averaged to produce a single mean scan, theoretically reducing the coordinate standard deviation of points to  $\pm 14\text{mm}$ .

### 3.3 Photogrammetric Results

Twenty-five photogrammetric targets were affixed to the face of the beam. Others were placed around the room and on stable components of the test frame. The photogrammetric coordination of the array of targets provided a common coordinate system for the TLS datasets. Photogrammetric data processing task was performed using *Australis* digital photogrammetric software (Fraser and Edmundson, 2000). The photogrammetric network was treated as a free network adjustment and the datum was defined by the stable targets. Several scale measurements were made using a steel band. The RMS of coordinate standard deviations of the targets was  $\pm 0.14\text{mm}$  ( $1\sigma$ ) and  $\pm 0.15\text{mm}$  ( $1\sigma$ ) for X and Y, respectively and  $\pm 0.04\text{mm}$  ( $1\sigma$ ) for Z, the most crucial direction for this experiment.

### 3.4 Scan Data Pre-Processing

Since both TLSs were set up at different positions, both scanners used the targets coordinated by the photogrammetric process to resect their relative positions and orientations. The dead load case for each TLS was used for this purpose. Once the resection parameters were derived, subsequent clouds were transformed into the photogrammetric coordinate system. A total of 11 control points were used for the Cyrax 2500 resection and 15 control points were used for the LMS-Z210 resection. Whilst the transformation process serves as an additional error source (Gordon and Lichti, 2004), it was a necessary task to enable direct comparisons of vertical deflections from the photogrammetric and TLS data sources.

Once all scan data were in the same reference frame, the individual scan clouds were manually edited to remove all scan points except for those on the top surface of the beam. The top of the beam was used for analysis because vertical deflection was the most pertinent for subsequent structural analyses. The extracted beam top clouds, though composed of irregularly spaced points, had an approximate sample interval of 5mm for the Cyrax 2500 and 15mm – 20mm for the LMS-Z210.

### 3.5 Beam Modelling

The timber beam conforms to the simply supported example shown in Figure 1. Therefore, Eq. 2 was adopted for this experiment. All TLS data for a single epoch were processed in one adjustment, thus simultaneously solving for the left ( $z_1$ ) and right ( $z_2$ ) models. The mean number of points used for each solution was 7364 for the Cyrax 2500 and 1099 for the LMS-Z210. Clearly, there were more observations available for the Cyrax 2500 dataset, which was a function of the smaller sampling interval offered by that TLS. The overall RMS of residuals from the least-squares adjustments was  $\pm 0.6\text{mm}$  for the Cyrax 2500 and  $\pm 5.4\text{mm}$  for the LMS-Z210. The difference in the size of residuals largely reflects the observational precision of each scanner. Statistical testing was performed on each parameter to determine its significance. If any parameters were found to be statistically insignificant, they would be eliminated and a new solution recomputed. In all cases there were no instances where parameters were found to be redundant.

### 3.6 Vertical Deflections

Vertical deflections were derived using the estimated models for each of the eight load epochs. The x and y coordinates of each of the 13 photogrammetric targets (constituting the top row of targets on the beam) were passed into the estimated models to compute a z-coordinate. Only the top row of targets was used because they were the closest to the beam top. The z-coordinates were then used to determine vertical deflections between epochs. Each TLS set of vertical deflections (i.e. for the Cyrax 2500 and the LMS-Z210) was compared to the vertical deflections produced by the photogrammetry and the differences are shown in Table 1.

Table 1 indicates that the estimated models using Cyrax 2500 data, compared to the benchmark photogrammetry, give an overall RMS of differences of  $\pm 0.29\text{mm}$ . The largest RMS of differences is  $\pm 0.47\text{mm}$  for the 15mm deflection case. The overall RMS of differences for the LMS-Z210 is  $\pm 3.6\text{mm}$ . The maximum RMS is  $\pm 5.0\text{mm}$  for the 25mm deflection case. The overall RMS values represent a factor of improvement (in precision) of 21 times for the Cyrax 2500 and 7 times for the LMS-Z210 over the coordinate precision of each TLS.

Nominal Vertical Deflection (mm)	RMS of Differences (mm)	
	Cyrax 2500	LMS-Z210
5	$\pm 0.12$	$\pm 3.6$
10	$\pm 0.14$	$\pm 4.1$
15	$\pm 0.47$	$\pm 3.2$
20	$\pm 0.26$	$\pm 2.3$
25	$\pm 0.24$	$\pm 5.0$
30	$\pm 0.27$	$\pm 5.0$
35	$\pm 0.30$	$\pm 2.7$
40	$\pm 0.34$	$\pm 1.4$
Total RMS	$\pm 0.29$	$\pm 3.6$

**Table 1:** RMS of differences between TLS-derived and photogrammetry-derived vertical deflections using 13 targets per deflection case

The linear term,  $a_{01}$ , was used to model rotation about the x-axis. In adjustments undertaken without the y-term, plots of residuals versus y-axis coordinates for the Cyrax 2500 shows a distinct tilt of approximately  $1.7^\circ$  and a tilt of  $2.7^\circ$  for the LMS-Z210 indicating that the beam top was not horizontal in the reference coordinate system for all cases. Analysis of the  $a_{01}$  parameter shows that it was consistently the same size for the Cyrax 2500 dataset ( $-0.030 \pm 0.001$ ) but fluctuated in the LMS-Z210 results ( $-0.047 \pm 0.017$ ). This was primarily due to the sparsity of data in the y-direction of the LMS-Z210 compared to the Cyrax 2500. The uncertainty in the determination of the  $a_{01}$  parameter caused vertical deflection measurements to be worse for the LMS-Z210 when compared to results where y-term was omitted (overall RMS of differences  $\pm 2.1\text{mm}$  for all cases where the y-term was omitted). Cyrax 2500 results were better with the y-term included and were worse without it (overall RMS of differences  $\pm 0.46\text{mm}$  without the y-term).

## 4. EXPERIMENT II: CONCRETE BEAM

The second major experiment conducted to test the analytical modelling strategy involved an 'L-shaped' (in cross section) 7.0m x 0.5m x 0.5m reinforced concrete beam that was loaded until failure. The beam was formerly part of an old bridge, which had been dismantled for the purpose of controlled laboratory testing. The beam was placed in a heavy-duty outdoor testing frame and supported at each end. The two load points were near the beam centre.

The beam was loaded in increments up to 240kN (approximately 13mm of vertical deflection), at which point the load was relaxed (epoch seven). This permitted the zero-datum of the contact sensors to be redefined. Loading resumed and continued in increments until the beam failed (490kN).

### 4.1 Set Up and Targeting

An LMS-Z210 was situated 7m from the beam and directly in front of the test frame (see Figure 2). It was set up as high as possible on the tripod enabling acquisition of points from the top surface of the beam. Similar to the first experiment, the position and orientation of the TLS was determined by resection. Photogrammetry was used to benchmark the experiment and the photogrammetric coordinate system provided the reference frame for the experiment.

### 4.2 Data Collection

A total of 13 measurement epochs were acquired during the period of testing. A dead load epoch was acquired at epoch zero and also at epoch seven (where the load on the beam was relaxed). The final measurement epoch where the beam was intact was epoch 12 but contact sensors were removed prior to this (after recording epoch 10) because failure was imminent. The impending specimen failure did not affect the remote measurement techniques (i.e. photogrammetry and TLS) highlighting, through practice, the advantage of a remote measurement technique. At each epoch, three repeat scans were collected and averaged to produce one mean scan.



**Figure 2:** Concrete beam and the Riegl LMS-Z210

### 4.3 Photogrammetric Results

Each photogrammetric epoch consisted of nine images from around the front of the beam ensuring strong convergent imaging angles. Photogrammetric adjustment was undertaken in a similar fashion to the timber beam experiment. The stable targets were used to define the datum in a free-network adjustment. Several scale measurements were acquired using a steel band. The RMS of the estimated coordinate precision of the photogrammetric targets was  $\pm 0.12\text{mm}$  ( $1\sigma$ ),  $\pm 0.21\text{mm}$  ( $1\sigma$ ) and  $\pm 0.09\text{mm}$  ( $1\sigma$ ) for X, Y and Z respectively.

### 4.4 Derivation and Adoption of Beam Deflection Models

Unlike the timber beam, the two load points used for the concrete beam experiment meant that it was divided into three sections. Figure 3 is a schematic diagram of the concrete beam.

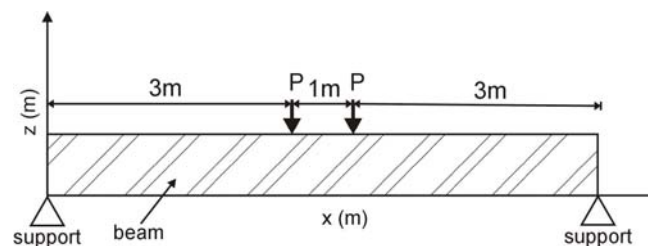


**Figure 3:** Schematic diagram for the concrete beam

The load points were situated 3m and 4m in from the left of the beam. Eq. 3 is the model adopted for the concrete beam. A y-term was included to cater for rotations about the x-axis in the concrete beam. Results indicated that the beam carried approximately  $1.5^\circ$  of rotation compared to the horizontal plane of the reference frame.

$$z(x) \begin{cases} z_1(x) = a_{30}x^3 + a_{10}x + a_{00} + a_{01}y & ; 0\text{m} \leq x \leq 3\text{m} \\ z_2(x) = b_{20}x^2 + b_{10}x + b_{00} + a_{01}y & ; 3\text{m} \leq x \leq 4\text{m} \\ z_3(x) = c_{30}x^3 + c_{20}x^2 + c_{10}x + c_{00} + a_{01}y & ; 4\text{m} \leq x \leq 7\text{m} \end{cases} \quad (3)$$

### 4.5 Analysis of the Adjustment

The overall RMS of residuals from all solutions was  $\pm 2.5\text{mm}$  for the least-squares estimation using a mean of 268 points. This is two times better than the fit of the timber beam models using the LMS-Z210 and most likely due to the extra terms of the concrete beam deflection functions making it more flexible when modelling the data. The mean value estimated for the y-term from all 12 load epochs was  $0.027 \pm 0.006$  (unitless). The beam top tilt, revealing itself as the gradient of the y-term, was more precisely determined than in the timber beam experiment.

## 4.6 Vertical Deflections

Computation of vertical deflections was undertaken in a similar fashion to the timber beam experiment. Planimetric coordinates of 12 photogrammetric targets were passed through the estimated models producing a height coordinate. The number of targets varied depending on their visibility in the photogrammetric images. Vertical deflections were computed by differencing the height coordinates. Table 2 shows the original differences for the entire 11-parameter model (Eq. 3). Statistical testing was performed to assess the significance of each parameter. Statistically redundant parameters were eliminated and the adjustment recomputed. The table includes the RMS of differences for the revised models and shows which parameters were eliminated.

The table indicates that the LMS-Z210 was achieving a measurement accuracy at the  $\pm 2.4\text{mm}$  level ( $1\sigma$ ). Testing the statistical significance of parameters and eliminating those whose contribution was scant permitted models to be alleviated of high parameter coupling though retaining their overall accuracy.

Epoch	Maximum vertical deflection (mm)	Number of Targets	11 parameter RMS (mm)	Revised model RMS (mm)	Eliminated parameters
1	2.1	12	$\pm 1.1$	$\pm 1.3$	$c_{30}$
2	4.1	12	$\pm 0.9$	$\pm 0.9$	
3	6.0	12	$\pm 3.7$	$\pm 3.7$	
4	8.0	12	$\pm 1.7$	$\pm 1.7$	$c_{30}$
5	10.0	12	$\pm 2.4$	$\pm 2.4$	
6	12.9	12	$\pm 2.3$	$\pm 2.1$	$c_{30}, a_{10}$
7	0.9	11	$\pm 2.1$	$\pm 2.1$	
8	4.1	12	$\pm 1.2$	$\pm 1.2$	
9	8.3	12	$\pm 2.0$	$\pm 2.1$	$c_{30}$
10	13.2	11	$\pm 3.2$	$\pm 2.8$	$c_{30}, a_{10}$
11	28.8	12	$\pm 2.7$	$\pm 2.8$	$c_{30}$
12	48.3	11	$\pm 3.3$	$\pm 3.5$	
	Total	RMS	$\pm 2.4$	$\pm 2.4$	

**Table 2:** Differences of vertical deflections between the LMS-Z210 and photogrammetry

## 5. TIMBER BRIDGE

A field trial was conducted involving an ageing timber bridge that was built prior to the 1950s (Figure 3). The bridge is located in Toodyay, Western Australia. It has experienced several repairs to reinforce its structure but it ended its operational life and has since been dismantled. Prior to disassembly, one span of the bridge was made available for structural testing. Testing involved placing large weights over a span and measuring the deformation at critical sites on the various structural members under the bridge.

TLS and photogrammetry were used to measure the spatial change occurring at the selected span. Photogrammetric targets were placed throughout the span. All targets, including a series of stable targets affixed to three horizontal steel beams, are visible in Figure 3.

For the purposes of testing the analytical modelling strategy (for TLS data), four timber stringers were used for analysis. A stringer is a horizontal beam with a cylindrical shape. Being timber logs cut from a local Wandoo and Jarrah forest, the diameter and straightness of a beam varies along its length. Their lengths were approximately 4m and their diameter approximately 400mm. The four stringers are visible in Figure 3 and are labelled 3-4 (at front), 3-3, 3-2 and 3-1 (at rear). The locations of photogrammetric targets, affixed to the stringers, are also visible along the bottom of each stringer.

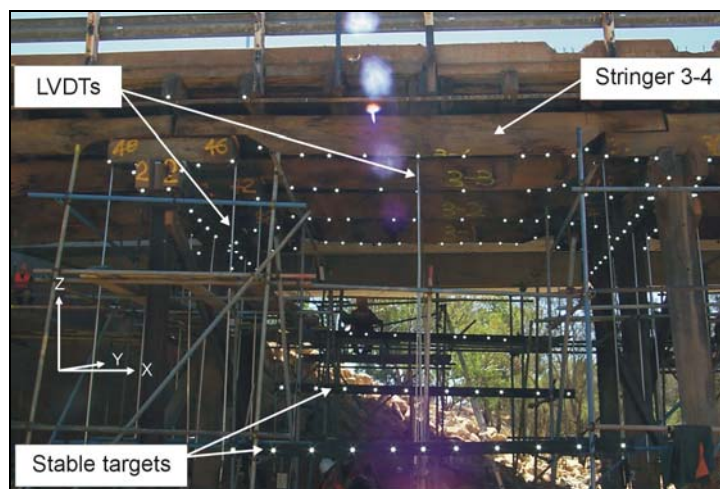


**Figure 3:** Span 3 of Toodyay Bridge

## 5.1 Set Up and Targeting

Photogrammetric targets were placed throughout the span. At least eight targets (and no more than ten) were available along the underside of each stringer. The targets were circular retroreflective stickers adhered to a black L-shaped metal bracket. Each bracket was fastened to the timber members using timber screws. Only targets placed on the underside of the stringer were used for analysis of vertical deflections in the ensuing computations.

## 5.2 Loading Schedule

The load was applied using a truck laden with concrete and steel weights. The amount of load and position of the truck on the bridge varied leading to a total of 95 different loading conditions on the day. A maximum of 60.65t was placed over the span. It is noted that with so many loading conditions and a great deal of time consumed in preparing the truck, very little time was available in which to capture the measurements. The time budgeted per epoch was two minutes. Of these 95 different loading conditions, only five are presented for analysis in the following sections. The remaining 90 test conditions were subtle variations of the five focused on here (*e.g.* altering the relative position of the truck on the bridge).

### 5.3 Data Collection

A Riegl LMS-Z210 TLS was placed 11m from the front of the bridge and directly between the span. It was set up over a known point and oriented towards another known point (these points were coordinated by a surveyor). The purpose of setting up over a known point was to enable the opportunity to return to the same position if episodic monitoring was required (it was unknown at the time if it was or not).

Of importance to the TLS set up was that the instrument was levelled. In the experiments presented in the previous two sections, it was assumed that the TLS was not levelled and analysis relied on 3D resection to determine the position and orientation of the scanner. Since the horizontal plane of the TLS was assumed to be coincident with the local project system (defined by the total station survey and subsequently adopted by the photogrammetry), a resection for the purpose of georeferencing the TLS need not take place.

With respect to the stringers, the TLS was positioned 11.6m from stringer 3-4 and 15.8m from stringer 3-1. Angles of inclination ranged from 15°15' to stringer 3-4 (at the front of the bridge) and 11°58' to stringer 3-1 (at the rear of the bridge). A single scan was captured per load epoch in the two minute window.

Photogrammetric data capture involved six convergent exposure stations around the front of the span. The camera was approximately 8m from the front of the bridge. Photographic data were exported from the camera to the on-site computer at regular intervals.

### 5.4 Photogrammetric Results

Approximate coordinates of some of the targets were computed by angle intersection using a pair of total stations. The coordination was necessary for the photogrammetric adjustment of all targets. Photogrammetric adjustment was undertaken using FEMBUN software (Lichti and Chapman, 1997). The object coordinate precision in the Z-axis (height dimension) was  $\pm 0.4$ mm for non-datum points.

The photogrammetric coordination of targets along the stringers revealed that the maximum vertical deflection (based on the greatest load applied during that day of testing) was approximately 8mm (for stringer 3-2). This is much less than the magnitude of vertical deflections encountered in the previous laboratory-based experiments.

### 5.5 Functional Modelling of Timber Stringer Deflection

Unlike the concrete and timber beams examined in the previous section, the timber stringers are most aptly described as beams supporting distributed loads. There is no specific load point (or load points) since the stringer bears the load of the truck, which is distributed by the members above it (*e.g.* bridge deck and bearers). Therefore, the load was assumed to be constant over the entire length of each stringer. In this case, the elastic curve of each stringer is described by a fourth-order linear differential equation (Beer and Johnston, 1992):

$$\frac{\partial^4 z}{\partial x^4} = -\frac{w(x)}{EI} \quad (4)$$

where  $EI$  are terms described previously and  $w(x)$  is the (uniformly distributed) load as a function of distance along the beam. The  $E$  and  $I$  terms were assumed to be constant though this was a loose assumption. **Figure** is a sketch for the distributed load,  $w$ , of each stringer.

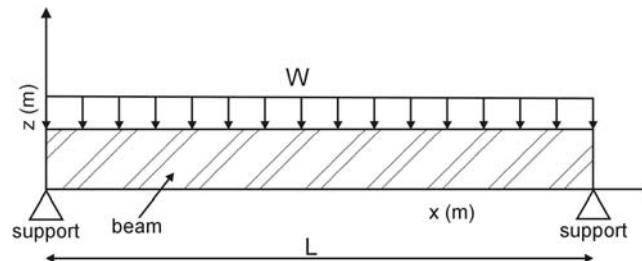


**Figure 4:** Schematic diagram for the Toodyay Bridge stringers

Integrating Eq. 4 four times with respect to  $x$  will yield the deflection equation:

$$EIz(x) = -\frac{1}{24} wx^4 + \frac{1}{12} wLx^3 + C_3x + C_4 \quad (5)$$

Simplifying and generalising the coefficients of Eq. 5 gives the final form of the analytical model representing the beam deflection adopted for the timber stringers:

$$z(x) = a_{40}x^4 + a_{30}x^3 + a_{10}x + a_{00} + a_{02}y^2 + a_{01}y \quad (6)$$

No explicit constraints were enforced since there was only one function describing the entire deflection of the stringer. Two terms were added to model trends in the  $y$ -direction. The laboratory-based experiments relied upon a single linear term but, due to the shape of the stringer, a quadratic term was also included. A quadratic term was selected because the stringer approximated a circular cross-section.

## 5.6 Analysis of the Adjustment

Table 4 shows the results for the least-squares estimation of the parameters of Eq. 6 for all four stringers for each load case. The number of point samples available on each stringer is also listed. The residuals are much higher than evident in previous experiments because of the physical shape of the stringer.

Load	Stringer 3-4		Stringer 3-3		Stringer 3-2		Stringer 3-1	
	Number of Points	RMS Residuals (m)						
0t	2371	±0.035	876	±0.024	646	±0.020	982	±0.046
41.2t	2385	±0.038	1099	±0.025	718	±0.022	992	±0.048
44.2t	2411	±0.038	1126	±0.024	811	±0.022	1132	±0.045
53.75t	2402	±0.038	1145	±0.025	809	±0.022	1121	±0.048
60.65t	2450	±0.039	1180	±0.025	823	±0.023	1126	±0.048
Mean	<b>2404</b>		<b>1085</b>		<b>761</b>		<b>1071</b>	
Total RMS (m)		<b>±0.038</b>		<b>±0.025</b>		<b>±0.022</b>		<b>±0.047</b>

**Table 4:** Results of least-squares estimation

## 5.7 Vertical Deflections

Vertical deflections were computed by differencing the photogrammetrically determined coordinates of the targets relative to the dead load. **Figure** shows the deflection vectors for all four stringers for the 60.65t load case (possessing the largest vertical deflections) using photogrammetric measurements. The vectors reveal a subtle bending where the deflections are slightly larger near the centre of the stringer.

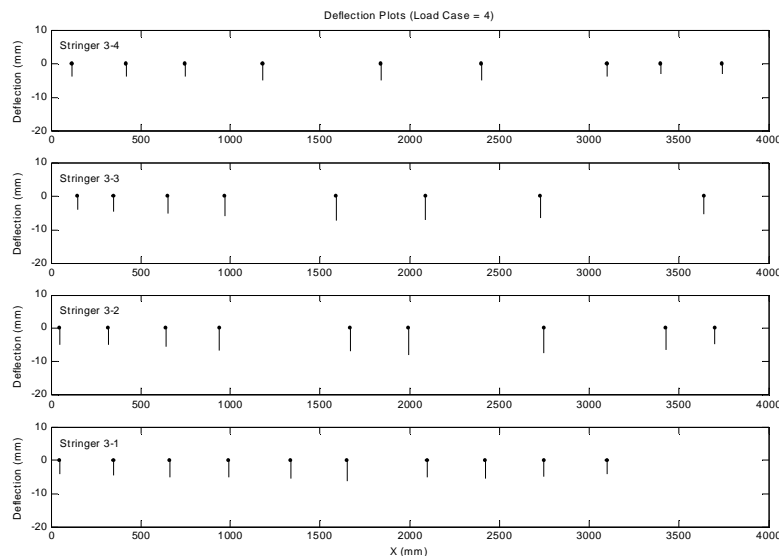


**Figure 5:** Vertical deflections computed from photogrammetry (60.65t load case)

TLS derived vertical deflections were computed using the estimated parameters of the analytical model. The x- and y-coordinates of each photogrammetric target was passed into the model yielding an estimated z-coordinate. Coordinate differencing was performed between the dead load and each subsequent load epoch. **Figure 1** shows the deflection vectors for each stringer for the fourth load case.

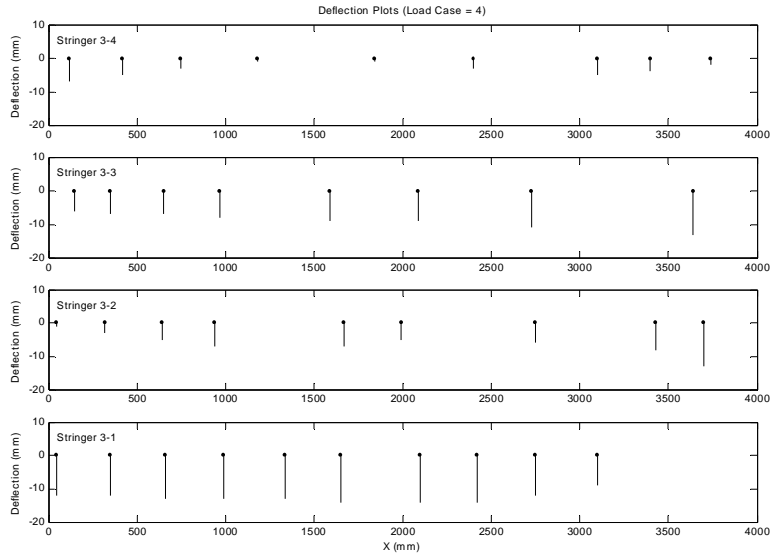


**Figure 1:** Vertical deflections computed from the TLS (60.65t load case)

There is no clear trend evident in Figure 6. Vertical deflections have been detected and the magnitude of the deflections for stringers 3-3 and 3-2 are of similar magnitude to that computed by photogrammetric means. A comparison of the TLS derived deflections and the photogrammetric derived deflections was performed. The comparisons were computed at the location of each target. The differences are shown in Table 5 along with the number of targets used along each stringer.

Stringer	RMS of Differences (mm) Load Case				Total RMS (mm)	Number of Targets
	1	2	3	4		
3-4	±4.3	±2.6	±3.7	±7.8	±5.0	9
3-3	±4.7	±3.2	±3.2	±3.3	±3.7	8
3-2	±7.2	±4.3	±4.3	±3.4	±5.0	9
3-1	±13.0	±8.4	±7.6	±11.0	±10.2	10

**Table 5:** Differences between photogrammetry and TLS vertical deflections

The RMS of differences range from ±2.6mm for the stringer closest to the TLS to ±13.0mm for the stringer furthest from the TLS. Overall, stringers 3-4, 3-3 and 3-2 consistently maintained the lowest differences compared to the photogrammetry and are at the same level of accuracy as the results presented in the previous two laboratory-based experiments. The vertical deflections for stringer 3-1 were the least accurately modelled and the RMS of differences represent an improvement of only two to three times the precision of the TLS. This stringer was the furthest from the TLS which is the most likely cause for the lack of accuracy. Given the computed accuracy of the TLS in this field case and the magnitude of vertical deflections encountered, the TLS has not been able to successfully measure the structural deformation. This is chiefly due to the instrument precision and also the strict

imaging constraints (i.e. one scan per epoch; other experiments permitted more scans per epoch).

## 6. CONCLUSIONS

An analytical modelling approach was developed to detect and measure vertical deformation. It involved representing the beam with a compound polynomial containing parameters that have a sound physical origin derived from first principles of beam deflection mechanics. This modelling avoids the arbitrary nature inherent in some other methods, such as gridding (Gordon et al., 2003a). The sub-millimetre results for the Cyra Cyrax 2500 place it in the same accuracy league as close-range photogrammetry (at least, for non-metric cameras). The perceived main advantage of photogrammetry over TLS is its high precision. The additional advantages of TLS, however, include full surface representation (as opposed to a few targets) and also a single set up geometry that does not have an inherently weak dimension (as photogrammetry has in depth). Furthermore, the reflectorless nature of TLS does not require targets except for validation.

## REFERENCES

- Beer, F. P. and Johnston, E. R. (1992) *Mechanics of Materials* (2nd Ed.), McGraw-Hill Book Company, Berkshire, England, 738 pp.
- Fraser, C. S. and Edmundson, K. L. (2000) Design and Implementation of a Computational Processing System for Off-Line Digital Close-Range Photogrammetry, *ISPRS Journal of Photogrammetry and Remote Sensing*, Vol. 55, No. 2, pp. 94 - 104.
- Gordon, S. J. and Lichti, D. D. (2004) Terrestrial Laser Scanners with a Narrow Field of View: The Effect on 3D Resection Solutions, *Survey Review*, Vol. 37, No. 292, pp. 448 - 468.
- Gordon, S. J., Lichti, D. D. and Stewart, M. P. (2003a) Structural Deformation Measurement using Terrestrial Laser Scanners, *Proceedings of 11th International FIG Symposium on Deformation Measurements*, Santorini Island, Greece, 25 - 28 May, p. 8.
- Gordon, S. J., Lichti, D. D., Chandler, I., Stewart, M. P. and Franke, J. (2003b) Precision Measurement of Structural Deformation using Terrestrial Laser Scanners, *Proceedings of Optical 3D Methods*, Zurich, Switzerland, 22 - 25 September, p. 8.
- Leica Geosystems (2004) *HDS2500 Description*, [http://www.cyra.com/products/HDS2500\\_description.html](http://www.cyra.com/products/HDS2500_description.html). Accessed: 14 June 2004.
- Lichti, D. D. (2004) A Resolution Measure for Terrestrial Laser Scanners, *Proceedings of ISPRS XX Congress*, Istanbul, Turkey, 12 - 23 July, p. 6.
- Lichti, D. D. and Chapman, M. A. (1997) Constrained FEM Self-Calibration, *Photogrammetric Engineering and Remote Sensing*, Vol. 63, No. 9, pp. 1111 - 1119.
- Riegl (2004) *3D Imaging Sensor LMS-Z210i*, [http://www.riegl.com/lms-z210i/e\\_lms-z210i.htm](http://www.riegl.com/lms-z210i/e_lms-z210i.htm). Accessed: 14 June, 2004.

## BIOGRAPHICAL NOTES

**Stuart Gordon** (B.Sc. (Hons.), Curtin) is a Ph.D. student with the Department of Spatial Sciences, Curtin University of Technology in Perth, Western Australia. His research focuses on terrestrial laser scanning. **Derek Lichti** holds B.Tech. in Survey Engineering from Ryerson University, Toronto, Canada, and M.Sc. and Ph.D. degrees in Geomatics Engineering from the University of Calgary, Canada. His research interests are in terrestrial laser scanning and close-range photogrammetry. **Jochen Franke** (Dipl.-Ing. (Karlsruhe), PGradDip (Surv&Mapp) (Curtin)) has been at the Department of Spatial Sciences since 2001 as a Research Associate in the field of applied terrestrial laser scanning. **Mike Stewart** holds a Ph.D. degree from the University of Edinburgh. He is Associate Professor of GPS at the Department of Spatial Sciences and his research focuses on deformation monitoring and GPS algorithm development.

## CONTACTS

Mr Stuart Gordon  
Western Australian Centre for Geodesy  
GPO Box U1987, WA, 6845, Perth  
AUSTRALIA  
Tel. + 61 8 9266 3505  
Fax + 61 8 9266 2703  
Email: S.Gordon@curtin.edu.au  
Web site: [www.cage.curtin.edu.au/lascan](http://www.cage.curtin.edu.au/lascan)